



UNIVERSITÀ POLITECNICA DELLE MARCHE
Repository ISTITUZIONALE

Effective Engineering Constants for Micropolar Composites with Imperfect Contact Conditions

This is the peer reviewed version of the following article:

Original

Effective Engineering Constants for Micropolar Composites with Imperfect Contact Conditions / Rodriguez-Ramos, R.; Yanes, V.; Espinosa-Almeyda, Y.; Sanchez-Valdes, C. F.; Otero, J. A.; Lebon, F.; Rizzoni, R.; Serpilli, M.; Dumont, S.; Sabina, F. J.. - 195:(2023), pp. 449-466. [10.1007/978-3-031-28744-2_19]

Availability:

This version is available at: 11566/327739 since: 2024-03-20T08:43:00Z

Publisher:

Springer, Cham

Published

DOI:10.1007/978-3-031-28744-2_19

Terms of use:

The terms and conditions for the reuse of this version of the manuscript are specified in the publishing policy. The use of copyrighted works requires the consent of the rights' holder (author or publisher). Works made available under a Creative Commons license or a Publisher's custom-made license can be used according to the terms and conditions contained therein. See editor's website for further information and terms and conditions.

This item was downloaded from IRIS Università Politecnica delle Marche (<https://iris.univpm.it>). When citing, please refer to the published version.

(Article begins on next page)

Effective engineering constants for micropolar composites with imperfect contact conditions

R. Rodríguez-Ramos, V. Yanes, Y. Espinosa-Almeyda, C. F. Sánchez-Valdés, F. Lebon, R. Rizzoni, M. Serpilli, S. Dumont, F. J. Sabina

Abstract

In this work, the homogenization theory is applied within the framework of three-dimensional linear micropolar media. The fundamental results derived by the asymptotic homogenization method to compute the effective engineering moduli for a laminated micropolar elastic composite with centro-symmetric constituents are

R. Rodríguez-Ramos

Facultad de Matemática y Computación, Universidad de La Habana, San Lázaro y L, Vedado, La Habana, CP 10400, Cuba, e-mail: reinaldo@matcom.uh.cu

V. Yanes

Escuela Técnica Superior de Ingeniería Aeronáutica y del Espacio, Universidad Politécnica de Madrid, Pza. Cardenal Cisneros 3, Madrid 28040, Madrid, España, e-mail: vh.yanes@upm.es

Y. Espinosa-Almeyda, C. F. Sánchez-Valdés,

Instituto de Ingeniería y Tecnología, Universidad Autónoma de Ciudad Juárez, Av. Del Charro 450 Norte Cd. Juárez, Chihuahua, CP 32310, México, e-mail: yoanhealmeyda1209@gmail.com; cesar.sanchez@uacj.mx

F. Lebon

Laboratoire de Mécanique et d'Acoustique, Université Aix-Marseille, CNRS, Centrale Marseille, CS 40006, 13453, Marseille Cedex 13, France, e-mail: lebon@lma.cnrs-mrs.fr

R. Rizzoni

Department of Engineering, University of Ferrara, Via Saragat 1, 44122, Ferrara, Italy

M. Serpilli

Department of Civil and Building Engineering, and Architecture, Università Politecnica delle Marche, Via Brecce Bianche, 60131, Ancona, Italy

S. Dumont

University of Nantes, Place Gabriel Péri, 30000 Nantes, France, e-mail: serge.dumont@unimes.fr

Federico J. Sabina

Instituto de Investigaciones en matemáticas Aplicadas y Sistemas, Universidad Nacional Autónoma de México, Apartado Postal 20-126, Alcaldía Álvaro Obregón, 01000, CDMX, México, e-mail: fjs@mym.iimas.unam.mx

summarized, in which the interface between the layer phases is considered imperfect spring type. The layers are considered with isotropic symmetry. Non-uniform and, as a particular case, uniform imperfections are assumed, where different imperfection parameters and cell length in the y_3 -direction are assigned for the analysis. The analytical expressions of the engineering constants related to the stiffness and torque are given as functions of the imperfection parameters. The behavior of the engineering coefficients depending on the imperfection is studied. The influence of the imperfection and the cell length in the direction of the imperfection is observed. The present study allows to validate other models and experimental results, as well as the investigation of fracture prediction in laminated composite materials.

1 Introduction

Several investigations in biomechanics have shown that models related to Cosserat-type media better capture the actual response of biological tissues [1, 2, 3, 4, 5]. The micromechanical study in Cosserat's media has had an impact on the mechanics of bones [6, 7, 8, 9, 10, 11, 12], cardiac tissues [13, 14], etc.

The applicability of laminated structures in various branches of industry is well known. The investigation of their properties is important to improve and design new materials. There are micromechanical methods based on multiscale homogenization schemes that provide information about the properties of heterogeneous laminated micropolar or Cosserat media, for example: Properties of micropolar multi-layered media have been calculated using the finite element technique [15, 16, 17]. In these works, the potentiality of the Cosserat continuum model to predict the mechanical behavior of layered structures is analyzed. Moreover, Cosserat continuum with 2D and 3D layered-like microstructure are analyzed by a finite element scheme in [18, 19]. On the other hand, multiscale homogenization approaches applied to micropolar heterogeneous structures have been carried out by [20, 21, 22, 23, 24, 25, 26], among others. In these approaches, the generalized stress and strain are linked to the displacements, strains, and stresses defined in the representative volume element.

Different works address the imperfect interface effects on multi-laminated media through the linear spring interface with zero thickness and the interphase models, [27, 28, 29, 30, 31, 32], among other. In the framework of heterogeneous micropolar or Cosserat elastic media, the problem of the existence of an imperfect interface between two contiguous phases have been considered. For example, the imperfect interface model applied to elastic composites [33, 34] is generalized to micropolar media assuming that the couple tractions are continuous across the interface and proportional to the jumps of the out-of-plane microrotation [35]. In addition, the boundary element method is used to simulate microstructured Cosserat media

with both perfect and uniform imperfect interfaces. The asymptotic analysis (see e.g. [36]) has proven to be a powerful mathematical tool to derive simplified models for thin films and structures [37, 38]. This technique has also been extensively used to study the mechanical behavior of layered composites, constituted by two solids bonded together by a thin interphase, considering different continuum theories with microstructure, such as micropolar elasticity [39], poroelasticity [40], and flexoelectricity [41]. Recently, the effective behavior of multi-laminated micropolar composites is studied using the asymptotic homogenization method [42, 43]. In both works, centro-symmetric cubic or isotropic constituents and perfect interface conditions are assumed. Other previous works dealing with the problem of imperfection in micropolar structures can be found in [44, 45, 46, 47]. Therefore, further analyses are required in this topic.

In the present work, based on the methodology presented in [42, 43, 48], the main results derived by the asymptotic homogenization method (AHM) to compute the effective engineering moduli for a laminated micropolar centro-symmetric composite are summarized, in which the interface between the layer phases is considered imperfect spring type. The layers are considered with isotropic symmetry. The imperfection is considered non-uniform and as a particular case uniform, controlled by different imperfection parameters and the cell length in the y_3 -direction. The analytical expressions of the effective engineering moduli associated to the stiffness and torque are given as a function of the non-uniform imperfect parameters. An analysis of the behavior of the effective engineering coefficients depending on the imperfection is performed. The influence of the imperfection and the cell length in the direction of the imperfection is observed.

2 Heterogeneous problem statement and fundamental equations

A periodic centro-symmetric linear elastic micropolar continuum Ω at the Cartesian coordinate system $\mathbf{x} = \{x_1, x_2, x_3\} \subset \mathbb{R}^3$ is defined by two independent sets of degrees of freedom given by the displacement $u_m(\mathbf{x})$ [m] and the microrotation $\omega_s(\mathbf{x})$ fields associated to each material point [49]. For the static case, it is formulated by the linear and angular balance equations

$$\begin{aligned} (C_{ijmn}(\mathbf{x}) e_{nm}(\mathbf{x}))_{,j} + f_i(\mathbf{x}) &= 0, \\ (D_{ijmn}(\mathbf{x}) \psi_{nm}(\mathbf{x}))_{,j} + \epsilon_{ijk} (C_{kjmn}(\mathbf{x}) e_{nm}(\mathbf{x})) + g_i(\mathbf{x}) &= 0, \end{aligned} \quad (1)$$

where $C_{ijmn}(\mathbf{x})$ [N/m²] is the stiffness tensor, $D_{ijmn}(\mathbf{x})$ [N] is the torque tensor, $f_i(\mathbf{x})$ [N/m³] are the body forces, and $g_i(\mathbf{x})$ [N/m²] are the body couples functions, with $i, j, k, m, n, s = 1, 2, 3$. The micropolar strain $e_{mn}(\mathbf{x})$ and the torsion-curvature

$\psi_{mn}(\mathbf{x})$ [m^{-1}] tensors are given by

$$e_{nm}(\mathbf{x}) = u_{m,n}(\mathbf{x}) + \epsilon_{mns}\omega_s(\mathbf{x}), \quad \psi_{nm}(\mathbf{x}) = \omega_{m,n}(\mathbf{x}), \quad (2)$$

where ϵ_{mns} is the Levi-Civita tensor, u_m is the displacement vector and ω_m is the microrotation vector, independent of the displacement. The notation $f_{,m} \equiv \partial f / \partial x_m$ and the square brackets contain the physical units of measure for the variable. In Eqs. (1) and (2), the symmetric part of $e_{nm}(\mathbf{x})$ corresponds to the classical strain tensor whereas its skew-symmetric part accounts for the local reorientation of the microstructure. Also, the symmetry conditions $C_{ijmn}(\mathbf{x}) = C_{mni j}(\mathbf{x})$ and $D_{ijmn}(\mathbf{x}) = D_{mni j}(\mathbf{x})$ are satisfied.

The system, Eq. (1), together with the boundary conditions on $\partial\Omega$

$$\begin{aligned} u_m(\mathbf{x})|_{\partial\Omega_1} = 0, \quad (C_{ijmn}(\mathbf{x})e_{nm}(\mathbf{x}))n_j|_{\partial\Omega_2} = F_i(\mathbf{x}), \\ \omega_m(\mathbf{x})|_{\partial\Omega_3} = 0, \quad (D_{ijmn}(\mathbf{x})\psi_{nm}(\mathbf{x}))n_j|_{\partial\Omega_4} = G_i(\mathbf{x}), \end{aligned} \quad (3)$$

where $F_i(\mathbf{x})$ and $G_i(\mathbf{x})$ are the surface body forces and moments, represent the static boundary value problem associated with the linear theory of micropolar elasticity whose coefficients are rapidly oscillating. In Eq. (3), n_j is the unit outer normal vector to $\partial\Omega$ and the subsets $\partial\Omega_i$ satisfy $\partial\Omega_i \cap \partial\Omega_j \neq \emptyset$ (disjoint sets) and $\partial\Omega = \bigcup_{i=1}^4 \partial\Omega_i$.

In addition to the problem statement (Eqs. (1)–(3)), we deal with the spring model described above considering imperfect contact conditions at the interface Γ , such as

$$\begin{aligned} (C_{ijmn}(\mathbf{x})e_{nm}(\mathbf{x}))n_j = K_{ij} \llbracket u_j \rrbracket, \quad \llbracket (C_{ijmn}(\mathbf{x})e_{nm}(\mathbf{x}))n_j \rrbracket = 0, \quad \text{on } \Gamma \\ (D_{ijmn}(\mathbf{x})\psi_{nm}(\mathbf{x}))n_j = Q_{ij} \llbracket \omega_j \rrbracket, \quad \llbracket (D_{ijmn}(\mathbf{x})\psi_{nm}(\mathbf{x}))n_j \rrbracket = 0, \quad \text{on } \Gamma \end{aligned} \quad (4)$$

where $\llbracket p \rrbracket = p^{(1)} - p^{(2)}$ means the jump of the function p across the interface Γ . K_{ij} [N/m^3] and Q_{ij} [N/m] are the extensional and microrotational imper-

fection parameters, such that $K_{ij} = \begin{pmatrix} K_t & 0 & 0 \\ 0 & K_s & 0 \\ 0 & 0 & K_n \end{pmatrix}$ and $Q_{ij} = \begin{pmatrix} Q_t & 0 & 0 \\ 0 & Q_s & 0 \\ 0 & 0 & Q_n \end{pmatrix}$. Here,

$K_t, K_s, K_n, Q_t, Q_s,$ and Q_n are the interface parameters in the normal and tangential directions, which are considered equals for the sake of simplicity as follows $K_t = K_s = K_n$ and $Q_t = Q_s = Q_n$. An equivalent form of the imperfect contact conditions (4) has been derived for soft micropolar interfaces in [39], by means of the asymptotic analysis.

3 Asymptotic homogenization method and effective engineering moduli for periodic laminated micropolar media

From now on, let us consider that the three-dimensional heterogeneous centrosymmetric linear elastic micropolar continuum Ω is described by a parallelepiped of dimensions l_i ($i = 1, 2, 3$) generated by repetitions of a periodic cell Y , whose layered direction is along the y_3 -axis. At the microscale, the transversal cross-section of Y is characterized by a bi-laminated composite in the plane Oy_2y_3 , see Fig. 1, where the constituent material phases are denoted by S_γ ($\gamma = 1, 2$) with volume V_γ , such as $Y = S_1 \cup S_2$, $S_1 \cap S_2 = \emptyset$, and $V_1 + V_2 = 1$. Imperfect contact conditions (uniform or non-uniform) are assumed at the interface region Γ between the layers following the Eq. (4).

The non-uniform imperfect interface is defined by partitioning Γ along the y_2 direction, where $\theta_r \ell_2$ is the length of the r -partition (denoted ${}^r\Gamma$) with imperfection length fraction θ_r ($r = 1, \dots, N$), ℓ_2 is the characteristic length of Y along the y_2 direction, and N is the number of partitions; such as, $\Gamma = \bigcup_{r=1}^N {}^r\Gamma$. In this context, K_{ij} and Q_{ij} are considered piecewise linear functions in each unit cell partition rY (with r fixed), such as

$${}^rY = \{ \mathbf{y} \in \mathbb{R}^3 : 0 < y_i < \ell_i, \text{ and } \sum_{s=0}^{r-1} \theta_s \ell_2 < y_2 < \sum_{s=1}^r \theta_s \ell_2, \theta_0 = 0 \} \text{ and } Y = \bigcup_{r=1}^N {}^rY. \text{ Also, } {}^r f = \begin{cases} {}^1 f & \text{in } {}^1 Y \\ \vdots \\ {}^N f & \text{in } {}^N Y \end{cases}, \text{ where } f \text{ might be replaced by } K_{ij} \text{ and } Q_{ij} \text{ or}$$

any function defined in rY . On the other hand, as a particular case, an uniform interface is taken into account when the values of the imperfection parameters in each cell partition rY are equals.

In this framework, the applied methodology based on the AHM for centrosymmetric micropolar composites with perfect contact conditions [42, 43] is implemented to the case of an imperfect interface. The AHM provides averaged expressions for the rapidly oscillating elasticity tensors of the original problem and proposes a homogeneous equivalent medium with the same behavior. Its main assumptions are that all fields are considered as power series of the small and positive definite dimensionless parameter ε whose coefficients are dependent on the macro (\mathbf{x}) and micro (\mathbf{y}) scales, see, for instance [50, 51, 52]. Both scales are related as $\mathbf{y} = \mathbf{x}/\varepsilon$, where $\varepsilon = \ell/L \ll 1$ is defined by the ratio between the characteristic size of the periodicity cell (ℓ) and the diameter of the body (L).

The AHM starts from the substitution of the expansions for the displacements $u_m^\varepsilon(\mathbf{x})$ and the microrotations $\omega_m^\varepsilon(\mathbf{x})$

$$u_m^\varepsilon(\mathbf{x}) = \sum_{\alpha=0}^{\infty} \varepsilon^\alpha u_m^{(\alpha)}(\mathbf{x}, \mathbf{y}), \quad \omega_m^\varepsilon(\mathbf{x}) = \sum_{\alpha=0}^{\infty} \varepsilon^\alpha \omega_m^{(\alpha)}(\mathbf{x}, \mathbf{y}), \quad (5)$$

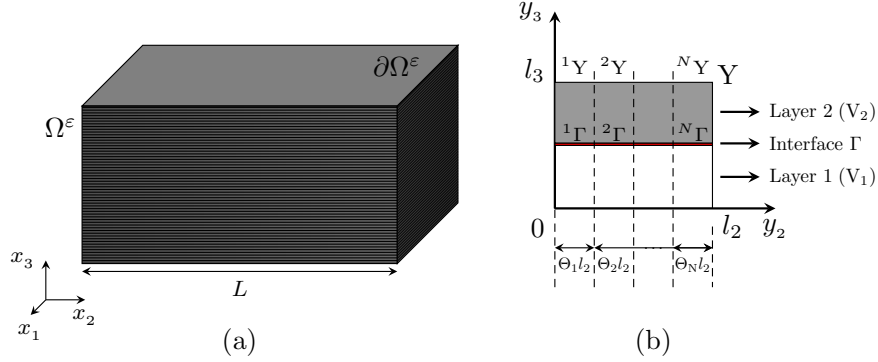


Fig. 1: (a) Heterogeneous Cosserat composite; (b) Cross-section of a periodic bilaminated structure Y at the plane Oy_2y_3 with non-uniform imperfect interface Γ partitioned in N disjoint sub-interfaces ${}^r\Gamma$ ($r = 1, 2, \dots, N$).

into the problem (Eqs. (1)–(4)), and following algebraic operations and differentiation rules. Here, $u_m^{(i)}(\mathbf{x}, \mathbf{y})$ and $\omega_m^{(i)}(\mathbf{x}, \mathbf{y})$ ($i = 0, 1, 2, \dots$) are infinitely differentiable and Y -periodic functions with respect to \mathbf{y} . Thus, a sequence of problems given by partial differential equations is obtained in relation to the power of ε parameter. From them, the formulation of local problems on Y , the effective moduli, and the equivalent homogenized problem with its asymptotic solution is obtained. Details about the AHM methodology related to micropolar laminated composites are shown in [23, 25, 42, 43] and are omitted here.

The mathematical statement of the ${}_{pq}{}^r\mathcal{L}^1$ and ${}_{pq}{}^r\mathcal{L}^2$ (with $p, q = 1, 2, 3$) local problems over each partition rY are given by

$${}_{pq}{}^r\mathcal{L}^1 \left\{ \begin{array}{l} (C_{i3pq} + C_{i3m3} {}^r_{pq}N'_m)' = 0, \quad \text{in } {}^rY \\ \llbracket C_{i3pq} + C_{i3m3} {}^r_{pq}N'_m \rrbracket n_3 = 0, \quad \text{in } {}^r\Gamma \\ (C_{i3pq} + C_{i3m3} {}^r_{pq}N'_m) n_3 = {}^rK_{ij} \llbracket {}^r_{pq}N_j \rrbracket, \quad \text{in } {}^r\Gamma \\ \langle {}^r_{pq}N_m \rangle_{rY} = 0, \end{array} \right. \quad (6)$$

$${}_{pq}{}^r\mathcal{L}^2 \left\{ \begin{array}{l} (D_{i3pq} + D_{i3m3} {}^r_{pq}M'_m)' = 0, \quad \text{in } {}^rY \\ \llbracket D_{i3pq} + D_{i3m3} {}^r_{pq}M'_m \rrbracket n_3 = 0, \quad \text{in } {}^r\Gamma \\ (D_{i3pq} + D_{i3m3} {}^r_{pq}M'_m) n_3 = {}^rQ_{ij} \llbracket {}^r_{pq}M_j \rrbracket, \quad \text{in } {}^r\Gamma \\ \langle {}^r_{pq}M_m \rangle_{rY} = 0, \end{array} \right. \quad (7)$$

where $(\bullet)' = d(\bullet)/dy_3$. In Eqs. (6) and (7), ${}^r_{pq}N_m$ and ${}^r_{pq}M_m$ are the local pq -displacements and pq -microrotations defined in the r -partition of the cell Y , respectively. The periodicity conditions ${}_{pq}N_m(0) = {}_{pq}N_m(l_i)$ and ${}_{pq}M_m(0) = {}_{pq}M_m(l_i)$

are satisfied and the unknown functions ${}^r_{pq}N_m$ and ${}^r_{pq}M_m$ only depend on y_3 as well.

The symbol $\langle p \rangle$ denotes the Voigt's average of the property p , i.e., $\langle p \rangle = \sum_{i=1}^N p^{(i)} V_i$

with N the number of phases in Y and $\sum_{i=1}^N V_i = 1$. In case of a bi-laminated composite, $\langle p \rangle = p^{(1)} V_1 + p^{(2)} V_2$ where $V_1 = \gamma/\ell_3$ and $V_2 = 1 - \gamma/\ell_3$ are the volume fractions per unit length occupied by the layer 1 and 2, respectively; such as, $V_1 + V_2 = 1$. γ is the y_3 coordinate of the constituents contact.

Once the unknown functions ${}^r_{pq}N_m$ and ${}^r_{pq}M_m$ are determined, the corresponding effective properties in terms of the r -interface-partition formulation can be found as follows:

$$C_{ijpq}^* = \sum_{r=0}^N \theta_r \langle C_{ijpq} + C_{ijm3} {}^r_{pq}N'_m \rangle_{rY}, \quad (8)$$

$$D_{ijpq}^* = \sum_{r=0}^N \theta_r \langle D_{ijpq} + D_{ijm3} {}^r_{pq}M'_m \rangle_{rY}. \quad (9)$$

The local functions ${}^r_{pq}N'_m$ and ${}^r_{pq}M'_m$ can be determined as it is shown in [42, 43] and after their replacement into Eq. (8), the corresponding stiffness and torque effective properties are obtained as functions of the constituent properties, the imperfection parameters and the constituent volume fraction

$$C_{ijpq}^* = \langle C_{ijpq} - C_{ijm3} C_{m3a3}^{-1} C_{a3pq} \rangle + \sum_{r=1}^N \theta_r \langle C_{ijm3} C_{m3a3}^{-1} \rangle (\langle C_{a3b3}^{-1} \rangle + \ell_3^{-1} {}^r K_{ab}^{-1})^{-1} \langle C_{b3c3}^{-1} C_{c3pq} \rangle, \quad (10)$$

$$D_{ijpq}^* = \langle D_{ijpq} - D_{ijm3} D_{m3a3}^{-1} D_{a3pq} \rangle + \sum_{r=1}^N \theta_r \langle D_{ijm3} D_{m3a3}^{-1} \rangle (\langle D_{a3b3}^{-1} \rangle + \ell_3^{-1} {}^r Q_{ab}^{-1})^{-1} \langle D_{b3c3}^{-1} D_{c3pq} \rangle. \quad (11)$$

Since both local problems (Eqs. (6) and (7)) and the effective properties (Eqs. (10) and (11)) have the same structure, only the analytical expressions for the stiffness are shown. The analytical expressions for effective torque moduli can be found replacing D for C , and Q for K .

3.1 Effective engineering moduli

Assuming that the constituents are centro-symmetric isotropic materials, these are characterized by 6 independent constants C_{1122} , C_{1212} , C_{1221} , D_{1122} , D_{1212} , and D_{1221} , see [53], through the relations

$$C_{ijmn} = C_{1122}\delta_{ij}\delta_{mn} + C_{1212}\delta_{im}\delta_{jn} + C_{1221}\delta_{in}\delta_{jm}, \quad (12)$$

$$D_{ijmn} = D_{1122}\delta_{ij}\delta_{mn} + D_{1212}\delta_{im}\delta_{jn} + D_{1221}\delta_{in}\delta_{jm}, \quad (13)$$

where δ_{ij} is the Kronecker delta tensor.

The global symmetry after the homogenization process is orthotropic, defined by eighteen non-zero effective moduli, as it is pointed out in [42, 43]. The nine non-zero stiffness effective properties are $C_{1111}^* = C_{2222}^*$, C_{3333}^* , C_{1122}^* , $C_{1133}^* = C_{2233}^*$, $C_{1313}^* = C_{2323}^*$, $C_{3232}^* = C_{3131}^*$, $C_{1331}^* = C_{2332}^*$, $C_{1212}^* = C_{2121}^*$, and C_{1221}^* . Similarly, the other nine torque properties can be derived.

Following the strain-stress relationships for a centro-symmetric micropolar media according to Eq. (1), and applying the effective relations reported in Eqs. (64)–(66) of [43] for the corresponding stiffness effective properties (see, Eq. (10)), the independent effective engineering moduli written as functions of the stiffness matrix components and the imperfection parameters are given as follows:

Effective Young's moduli:

$${}_sE_1^* = {}_sE_2^* = \frac{\left(\langle C_{1111} \rangle - \langle C_{1122} \rangle\right) \left(\langle C_{1111} \rangle + \langle C_{1122} \rangle - 2 \langle C_{1122}^2 C_{1111}^{-1} \rangle\right)}{\langle C_{1111} \rangle - \langle C_{1122}^2 C_{1111}^{-1} \rangle}, \quad (14)$$

$${}_sE_3^* = \frac{\left(\langle C_{1111} \rangle + \langle C_{1122} \rangle - 2 \langle C_{1122}^2 C_{1111}^{-1} \rangle\right) B_1({}^rK_{33})}{\langle C_{1111} \rangle + \langle C_{1122} \rangle - 2 \langle C_{1122}^2 C_{1111}^{-1} \rangle + 2 \langle C_{1122} C_{1111}^{-1} \rangle^2 B_1({}^rK_{33})}.$$

Effective shear moduli:

$${}_sG_{12}^* = {}_sG_{21}^* = \frac{\langle C_{1212} \rangle^2 - \langle C_{1221} \rangle^2}{\langle C_{1212} \rangle},$$

$${}_sG_{13}^* = {}_sG_{23}^* = \frac{\left(\langle C_{1212} \rangle - \langle C_{1221}^2 C_{1212}^{-1} \rangle\right) B_2({}^rK_{22})}{\langle C_{1212} \rangle - \langle C_{1221}^2 C_{1212}^{-1} \rangle + \langle C_{1221} C_{1212}^{-1} \rangle^2 B_2({}^rK_{22})}, \quad (15)$$

$${}_sG_{32}^* = {}_sG_{31}^* = \langle C_{1212} \rangle - \langle C_{1221}^2 C_{1212}^{-1} \rangle.$$

Effective Poisson's ratios:

$${}_s\nu_{21}^* = \frac{\langle C_{1122}^2 C_{1111}^{-1} \rangle - \langle C_{1122} \rangle}{\langle C_{1122}^2 C_{1111}^{-1} \rangle - \langle C_{1111} \rangle},$$

$${}_s\nu_{32}^* = {}_s\nu_{31}^* = \frac{\langle C_{1122} C_{1111}^{-1} \rangle B_1({}^rK_{33})}{\langle C_{1111} \rangle + \langle C_{1122} \rangle - 2 \langle C_{1122}^2 C_{1111}^{-1} \rangle + 2 \langle C_{1122} C_{1111}^{-1} \rangle^2 B_1({}^rK_{33})}. \quad (16)$$

Effective shear-strain ratios:

$${}_s\zeta_{2112}^* = \frac{\langle C_{1221} \rangle}{\langle C_{1212} \rangle}, \quad {}_s\zeta_{3223}^* = \langle C_{1221} C_{1212}^{-1} \rangle, \quad (17)$$

where the following parameters $B_1({}^r K_{33})$ and $B_2({}^r K_{22})$ are introduced for better presentation of the formulae

$$\begin{aligned} B_1({}^r K_{33}) &= \sum_{r=1}^N \theta_r \left(\langle C_{1111}^{-1} \rangle + \frac{1}{\ell_3} {}^r K_{33}^{-1} \right)^{-1}, \\ B_2({}^r K_{22}) &= \sum_{r=1}^N \theta_r \left(\langle C_{1212}^{-1} \rangle + \frac{1}{\ell_3} {}^r K_{22}^{-1} \right)^{-1}. \end{aligned} \quad (18)$$

The effective engineering constants for torque moduli can be written in analogous form and they are denoted by a subscript T , for example: the torsional Young's moduli ${}^r E_i^*$, the torsional shear moduli ${}^r G_{12}^*$, ${}^r G_{13}^*$ and ${}^r G_{32}^*$, the twist Poisson's coefficient ${}^r \nu_{21}^*$ and ${}^r \nu_{32}^*$, and the twist shear-strain ratios ${}^s \zeta_{2112}^*$ and ${}^s \zeta_{3223}^*$.

4 Numerical results

In this section, the Eqs. (14)-(18) are implemented to analyze the effect of a non-uniform or uniform imperfect interface Γ on the effective engineering moduli of a centro-symmetric bi-laminated Cosserat composite (layer 1/layer 2 = SyF/PUF) with isotropic constituents. The values of the Cosserat elastic parameters listed in Table 1 are used for computations through the relations $C_{1122} \equiv \lambda$, $(C_{1212} + C_{1221})/2 \equiv \mu$, $(C_{1212} - C_{1221})/2 \equiv \alpha$, $D_{1122} \equiv \beta$, $(D_{1212} + D_{1221})/2 \equiv \gamma$, and $(D_{1212} - D_{1221})/2 \equiv \epsilon$, where λ and μ are the Lamé parameters, α is the micropolar couple modulus, and the properties β , γ , and ϵ represent the additional micropolar elastic constants introduced in micropolar theory, according to the following constitutive law for a micropolar isotropic centro-symmetric material:

$$\begin{aligned} \sigma_{ij} &= (\mu + \kappa)e_{ij} + (\mu - \kappa)e_{ji} + \lambda e_{kk}\delta_{ij}, \\ \chi_{ij} &= (\gamma + \beta)\psi_{ij} + (\gamma - \beta)\psi_{ji} + \alpha\psi_{kk}\delta_{ij}, \end{aligned} \quad (19)$$

where σ_{ij} and χ_{ij} represent the stress and couple-stress tensors components, respectively. These materials data are taken from [53]. For the micropolar constants, the same notation of [53] is used, being α is κ , β is α , γ remains γ , and ϵ is β .

Table 1: Constituent material properties. ^a Syntactic foam - hollow glass spheres in epoxy resin, and ^b Dense polyurethane foam

Material properties	λ (MPa)	μ (MPa)	α (MPa)	β (N)	γ (N)	ϵ (N)
SyF ^a	2097.0	1033.0	114.8	-2.91	4.364	-0.133
PUF ^b	762.7	104.0	4.333	-26.65	39.98	4.504

Non-uniform imperfect interface

Here, the non-uniform imperfect interface Γ is defined by a partition of N disjoint sub-interfaces ${}^r\Gamma$ characterized by an imperfection length fraction ${}^r\theta$ and by two sets of imperfection parameters (${}^rK_{ij}$ and ${}^rQ_{ij}$) with a considerably large gap between their values for each partition, see Section 3.

In Table 3, the effective engineering moduli related to the stiffness (${}_sE_3^*$, ${}_sG_{13}^*$, ${}_s\nu_{31}^*$) and torques (${}_rE_3^*$, ${}_rG_{13}^*$, ${}_r\nu_{31}^*$) affected by the imperfection are shown for four SyF volume fraction (V_1) equals to 0.2, 0.4, 0.6, and 0.8. Two different partitions of Γ are analyzed, one with $N = 2$ partitions and another with $N = 4$ partitions. In the case of $N = 2$, $\theta_1 = \theta_2 = 0.5$ and the corresponding imperfection parameters are defined by ${}^rK_{ij}$ and ${}^rQ_{ij}$ ($r = 1, 2$), whereas, for $N = 4$, $\theta_1 = \theta_2 = \theta_3 = \theta_4 = 0.25$ and the imperfection parameters are ${}^rK_{ij}$ and ${}^rQ_{ij}$ ($r = 1, \dots, 4$) with $ij = 22, 33$. For both partitions, three different sets of imperfection parameters (S_1, S_2 and S_3) are considered for ${}^rK_{ij}$ and ${}^rQ_{ij}$, see Table 2. For example, when $N = 2$, S_1 is the set of values ${}^1K_{ij} = 10^{-1}$, ${}^2K_{ij} = 10^0$, ${}^1Q_{ij} = 10^{-1}$, and ${}^2Q_{ij} = 10^0$. The remaining sets can be understood in similar form. The characteristic lengths of Y along the x_2 and x_3 directions are $\ell_3 = 10^{-6}$ m and $\ell_2 = 1$, respectively. In addition, the effective values associate to the perfect contact case are reported for the same volume fractions.

From Table 3, it can be observed that the influence of the non-uniform imperfect interface is remarkable in the effective engineering properties, regardless of the V_1 volume fraction, and even the microstructure of the imperfection region determined by the partition N affects the behavior of the properties. A non-uniform interface with values for ${}^rK_{ij}$ and ${}^rQ_{ij}$ as in S_1 or lower implies the delamination of the material, and hence, a loss of the effective properties. However, as the values of the imperfection parameters increase as in S_2 and S_3 , an approach to the existence of a perfect interface is appreciated, and then the engineering moduli have an increment. The perfect contact is reached when the values of ${}^rK_{ij}$ and ${}^rQ_{ij}$ parameters are 10^{14} in each ${}^r\Gamma$. The highest values of the engineering constants are achieved in this perfect case. Furthermore, it can be seen that the effect of the imperfection is more noticeable in the engineering moduli related to compliance (${}_sE_3^*$, ${}_sG_{13}^*$, ${}_s\nu_{31}^*$) than

those related to torque (${}_{\tau}E_3^*$, ${}_{\tau}G_{13}^*$, ${}_{\tau}V_{31}^*$), and is even more pronounced for high SyF volume fraction. As N increases, the micro-structure of the imperfection becomes finer and its effect on the constant engineering behaviors is evident.

On the other hand, in Table 4, the remaining effective engineering moduli, which are independent of the imperfection effect, are reported for four SyF volume fractions ($V_1 = 0.2, 0.4, 0.6, \text{ and } 0.8$). As can be seen in Eqs. (14)-(18), these effective moduli only depend on the material constituents and their volume fraction, therefore, their behaviors are related to the hardness or softness of the SyF material properties. According to Table 1, we can see that SyF is harder than PUF. Thus, for the perfect case, as V_1 volume fraction increases, the effective engineering constants ${}_sE_1^*$, ${}_sE_3^*$, ${}_sG_{13}^*$, ${}_sG_{12}^*$ and ${}_sG_{31}^*$ for compliance and the other ones ${}_{\tau}\zeta_{2112}^*$ and ${}_{\tau}\zeta_{3223}^*$ for torques increase too. The opposite happens for the remaining Cosserat elastic parameters, which are softer for SyF and thus for the composite as V_1 increases. The effective engineering constants are stiffer in this case.

Table 2: Sets of values for the ${}^rK_{ij}$ and ${}^rQ_{ij}$ imperfection parameters considered in each partition of ${}^r\Gamma$.

Set	$N = 2$				$N = 4$							
	${}^1K_{ij}$	${}^2K_{ij}$	${}^1Q_{ij}$	${}^2Q_{ij}$	${}^1K_{ij}$	${}^2K_{ij}$	${}^3K_{ij}$	${}^4K_{ij}$	${}^1Q_{ij}$	${}^2Q_{ij}$	${}^3Q_{ij}$	${}^4Q_{ij}$
S_1	10^3	10^4	10^1	10^2	10^3	10^4	10^5	10^6	10^1	10^2	10^3	10^4
S_2	10^5	10^6	10^3	10^4	10^5	10^6	10^7	10^8	10^3	10^4	10^5	10^6
S_3	10^7	10^8	10^5	10^6	10^7	10^8	10^9	10^{10}	10^5	10^6	10^7	10^8

Table 3: Variation of the effective engineering moduli related to non-uniform imperfect interface for four SyF volume fraction (V_1). The moduli ${}_sE_3^*$, ${}_sG_{13}^*$ are measured in [MPa]; ${}_\tau E_3^*$, ${}_\tau G_{13}^*$ in [N]; ${}_s\nu_{31}^*$, ${}_\tau\nu_{31}^*$ are dimensionless.

Moduli	V_1	$N = 2$			$N = 4$			Perfect
		S_1	S_2	S_3	S_1	S_2	S_3	
${}_sE_3^*$	0.2	0.0055*	0.5493	48.8405	0.2774	25.1987	307.7864	581.9802
	0.4	0.0055*	0.5495	50.4403	0.2775	25.7829	392.7140	853.5091
	0.6	0.0055*	0.5496	51.5785	0.2776	26.2485	489.5963	1194.0030
	0.8	0.0055*	0.5497	52.5544	0.2776	26.6766	626.0288	1719.9066
${}_sG_{13}^*$	0.2	0.0055*	0.5437	25.9370	0.2752	14.7569	47.3517	62.7962
	0.4	0.0055*	0.5457	31.2829	0.2759	17.0148	67.8537	97.8025
	0.6	0.0055*	0.5470	35.9172	0.2765	19.1634	92.8556	142.0619
	0.8	0.0055*	0.5481	41.0084	0.2770	21.6470	135.7580	218.5210
${}_s\nu_{32}^*$	0.2	3.2×10^{-6}	3.2×10^{-4}	0.0283	2×10^{-4}	0.0146	0.1785	0.3376
	0.4	1.9×10^{-6}	1.9×10^{-4}	0.0171	9×10^{-5}	0.0088	0.1335	0.2901
	0.6	1.3×10^{-6}	1.3×10^{-4}	0.0118	6×10^{-5}	0.0060	0.1117	0.2724
	0.8	0.9×10^{-6}	0.9×10^{-5}	0.0086	5×10^{-5}	0.0044	0.1024	0.2813
${}_\tau E_3^*$	0.2	6×10^{-5} *	0.0044	0.0219	0.0025	0.0210	0.0227	0.0228
	0.4	6×10^{-5} *	0.0041	0.0151	0.0024	0.0147	0.0155	0.0156
	0.6	6×10^{-5} *	0.0033	0.0083	0.0021	0.0081	0.0084	0.0084
	0.8	5×10^{-5} *	0.0010	0.0012	0.0008	0.0012	0.0012	0.0012
${}_\tau G_{13}^*$	0.2	6×10^{-5} *	0.0055*	0.5043	0.0028*	0.2585	3.9585	8.2248
	0.4	6×10^{-5} *	0.0055*	0.4800	0.0028*	0.2477	2.7316	5.1540
	0.6	6×10^{-5} *	0.0055*	0.4512	0.0028*	0.2360	1.9728	3.3367
	0.8	6×10^{-5} *	0.0055*	0.3998	0.0028*	0.2179	1.2555	1.7927
${}_\tau\nu_{32}^*$	0.2	-0.0024	-0.1943	-0.9585	-0.1085	-0.9211	-0.9964	-0.9990
	0.4	-0.0035	-0.2605	-0.9704	-0.1511	-0.9432	-0.9965	-0.9987
	0.6	-0.0065	-0.3955	-0.9833	-0.2483	-0.9677	-0.9975	-0.9989
	0.8	-0.0439	-0.8207	-0.9973	-0.6981	-0.9949	-0.9994	-0.9996

* The values with more significant digits are given in Appendix A.

Table 4: Effective engineering moduli calculated for four SyF volume fraction V_1 . The moduli ${}_sE_1^*$, ${}_sG_{12}^*$ and ${}_sG_{31}^*$ are measured in [MPa]; ${}_\tau E_1^*$, ${}_\tau G_{12}^*$ and ${}_\tau G_{31}^*$ in [N]; and the others ${}_s\nu_{21}^*$, ${}_s\zeta_{2112}^*$, ${}_s\zeta_{3223}^*$, ${}_\tau\nu_{21}^*$, ${}_\tau\zeta_{2112}^*$, and ${}_\tau\zeta_{3223}^*$ are dimensionless.

V_1	${}_sE_1^*$	${}_sG_{12}^*$	${}_sG_{31}^*$	${}_s\nu_{21}^*$	${}_s\zeta_{2112}^*$	${}_s\zeta_{3223}^*$
0.2	793.4487	96.8720	95.9654	0.3690	0.8329	0.8960
0.4	1285.0272	176.1125	175.2921	0.3510	0.8149	0.8720
0.6	1776.1720	255.2062	254.6187	0.3427	0.8071	0.8480
0.8	2267.1612	334.2504	333.9454	0.3380	0.8027	0.8240
V_1	${}_\tau E_1^*$	${}_\tau G_{12}^*$	${}_\tau G_{31}^*$	${}_\tau\nu_{21}^*$	${}_\tau\zeta_{2112}^*$	${}_\tau\zeta_{3223}^*$
0.2	0.0228	12.9020	12.8438	-0.9997	0.8037	0.8506
0.4	0.0156	9.6077	9.4956	-0.9997	0.8133	0.9036
0.6	0.0084	6.3040	6.1475	-0.9998	0.8306	0.9567
0.8	0.0012	2.9721	2.7994	-0.9999	0.8706	1.0098

Uniform imperfect interface

Now, the effect of an uniform imperfect interface on the effective engineering moduli is analyzed. The uniform imperfect interface is defined as a particular case of the previously described non-uniform imperfect ones assuming that the values of ${}^rK_{ij}$ and ${}^rQ_{ij}$ imperfection parameters are the same along Γ , such as $K \equiv {}^rK_{ij}$ and $Q \equiv {}^rQ_{ij}$.

The numerical simulations are conducted for different grades of imperfection, such as the values for K are 10^6 , 5×10^6 , 10^7 , 3×10^7 , 5×10^7 , 10^8 , and the latest 10^{10} (Perfect contact); and for Q are 10^5 , 2×10^5 , 3×10^5 , 5×10^5 , 10^6 , 5×10^6 , and finally 10^7 (Perfect contact), respectively. Also, the characteristic lengths $\ell_3 = 10^{-4}$ and $\ell_2 = 1$.

In Figs. 2 and 3, only the behaviors of the effective engineering moduli affected by the imperfection are illustrated for a bi-laminated Cosserat composites (SyF/PUF) versus SyF volume fraction considering different imperfect parameters. We remark that these effective engineering moduli are sensitive to the imperfection, that is, they get weaker and only reach their highest values in the case of perfect contact. Notice that ${}_sE_3^*$, ${}_sG_{13}^*$, and ${}_s\nu_{32}^*$ are more sensitive to the imperfection K when V_1 increases whereas ${}_\tau G_{13}^*$, and ${}_\tau\nu_{32}^*$ have the same performance for Q when low values of V_1 is attached. However, ${}_\tau E_3^*$ undergoes slight changes caused by the effect of the Q imperfection. In this sense, a zoom illustrates the slight weakening of the property

when V_1 is closed to 0.4. Despite the imperfection effect, the ${}_sE_3^*$ and ${}_sG_{13}^*$ become stronger as V_1 increase whereas the opposite occurs for ${}_T E_3^*$ and ${}_T G_{13}^*$.

On the other hand, it is remarkable the behavior of the effective Poisson ${}_s\nu_{32}^*$ and twist Poisson ${}_T\nu_{32}^*$ moduli. The module ${}_s\nu_{32}^*$ has a concave upward behavior whereas ${}_T\nu_{32}^*$ is concave downward for all ${}^rK_{ij}$ and ${}^rQ_{ij}$ imperfection parameters in the whole V_1 interval. Also, ${}_s\nu_{32}^*$ is positive and ${}_T\nu_{32}^*$ is negative. These behaviors are similar to the one reported by Ref. [54] for an elastic solid weakened by porosity and microcracks. Paraphrasing his statement 4 from the conclusions [54], the Poisson and twist Poisson moduli can increase, decrease or remain unchanged depending on the imperfection parameters and the SyF volume fraction. The trend of the plots is reversed by passing from Fig. 2 to Fig. 3, they are mirror-like. This can be understood by looking at the values in Table 1, the elastic coefficients are larger for SyF; but the opposite happens for the micropolar constants, they are larger for PUF.

Notice the existence of a change correlation point for ${}_T\nu_{32}^*$ in $V_1 = 0.8333087$ (Fig. 3). This point is a consequence of $\langle D_{1111} \rangle + \langle D_{1122} \rangle - 2\langle D_{1122}^2 D_{1111}^{-1} \rangle = 0$ in Eq. (16) for the torque. Thus, ${}_T\nu_{32}^* = {}_T\nu_{31}^* = 0.5\langle D_{1122} D_{1111}^{-1} \rangle^{-1} \equiv H(V_1)$. All the curves are intercepted in this correlation point and $H(V_1)$ shows the independence of ${}_T\nu_{32}^*$ with respect to ${}^rQ_{ij}$. Moreover, it is worth mentioning that the computed values for ${}_sE_3^*$ and ${}_s\nu_{32}^*$ in Fig. 3 are comparable with those obtained experimentally in [53]. Indeed, the experimental values for the torsional micropolar Young's modulus and twist Poisson's ratio are, respectively, equal to 0 and -1. The slight difference, highlighted in the present plots, is likely due to the presence of the interface and to numerical approximations.

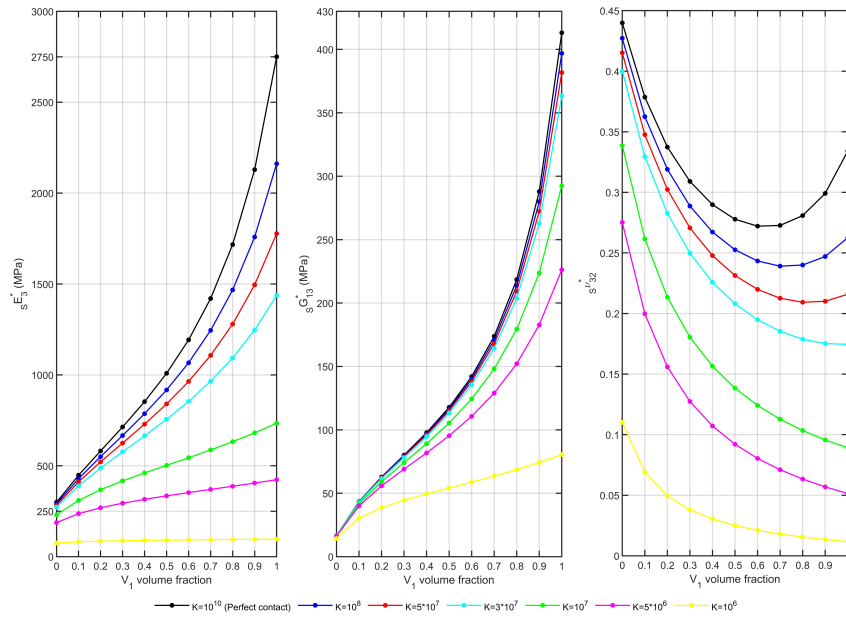


Fig. 2: Effective engineering moduli (${}_sE_{33}^*$, ${}_sG_{13}^*$, and ${}_sv_{32}^*$) related to stiffness versus V_1 volume fraction of a bi-laminated Cosserat composite with uniform imperfect contact conditions.

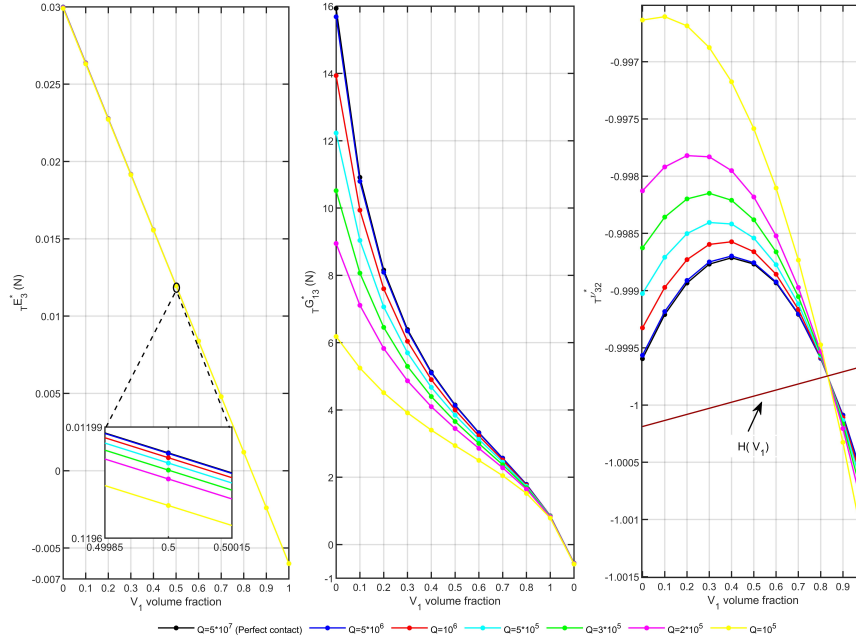


Fig. 3: Effective engineering moduli (tE_3^* , tG_{13}^* , and $t\nu_{32}^*$) related to torque versus V_1 volume fraction of a bi-laminated Cosserat composite with uniform imperfect contact conditions.

Conclusions

In this work, the asymptotic homogenization method is applied to heterogeneous micropolar media. In particular, the effective engineering expressions with isotropic symmetry layers are provided for multi-laminated Cosserat media under non-uniform imperfect contact conditions. The effective engineering properties for centro-symmetric laminated Cosserat composites are derived as a function of the material properties, the imperfection parameters, the cell length in the y_3 direction, and the constituent's volume fractions. The typical length scales of the periodic cell and the microstructure imperfection play an important role in the macroscopic behavior of the laminate structures. The homogenized Cosserat engineering constants are characterized by two effective Young's moduli, three effective shear moduli, two effective Poisson's ratios and two effective shear-strain ratios. Actually, only the transverse properties perpendicular to the layers distribution, i.e. along the x_3

depends on the imperfection parameter. Finally, numerical results are discussed. In general, we conclude that:

(i) The stiffness $({}_sE_3^*, {}_sG_{13}^*, {}_s\nu_{31}^*)$ and torque $({}_tE_3^*, {}_tG_{13}^*, {}_t\nu_{31}^*)$ effective engineering constants transverse to the distribution of the laminae are sensible to the imperfection effects;

(ii) The effective engineering constants related to stiffness and torque, i.e. Young's moduli $E_1^* = E_2^*$, shear moduli $G_{12}^* = G_{21}^*$, $G_{32}^* = G_{31}^*$, Poisson's coefficient ν_{21}^* , shear-strain ratios ζ_{2112}^* and ζ_{3223}^* are independent of the imperfection parameters and the cell length;

(iii) The volume fraction has an influence on the behavior of the stiffness and torque effective engineering moduli when the imperfect contact is considered, and;

(iv) The cell length changes the effective engineering constants when imperfect contact conditions are assumed.

Acknowledgements YEA gratefully acknowledges the financial support of Grant A1-S-37066 during the postdoctoral stay at IIT, UACJ. CFSV is grateful for the support of the CONACYT Basic Science Grant A1-S-37066. VY is grateful for the support and funding of the XS-Meta project during the course of his PhD. FJS and RRR acknowledge the funding of PAPIIT-DGAPA-UNAM IN101822, 2022-2023. This work was partially written during the visit of RRR at Aix-Marseille University, Centrale Marseille, the LMA-CNRS, and the University of Ferrara 2022. RRR thanks to co-funding of the Departmental Strategic Plan, Department of Engineering, University of Ferrara. This work is devoted to Igor Sevostianov, who apported significant contributions in the micro-mechanic area.

Appendix

The corresponding full approximation values with more significant digits of the effective engineering moduli ${}_sE_3^*$, ${}_sG_{13}^*$, ${}_tE_3^*$, and ${}_tG_{13}^*$ labeled with the symbol “*” in Table 3 are given.

Table 5: The values with more significant digits of the effective engineering moduli. The moduli ${}_sE_3^*$ and ${}_sG_{13}^*$ are measured in [MPa]; ${}_tE_3^*$, and ${}_tG_{13}^*$ in [N]

Moduli	V_1	$N = 2$		$N = 4$
		S_1	S_2	S_1
${}_sE_3^*$	0.2	0.00549993	–	–
	0.4	0.00549995	–	–
	0.6	0.00549996	–	–
	0.8	0.00549997	–	–
${}_sG_{13}^*$	0.2	0.00549937	–	–
	0.4	0.00549957	–	–
	0.6	0.00549970	–	–
	0.8	0.00549981	–	–
${}_tE_3^*$	0.2	5.48674×10^{-5}	–	–
	0.4	5.48063×10^{-5}	–	–
	0.6	5.46415×10^{-5}	–	–
	0.8	5.25861×10^{-5}	–	–
${}_tG_{13}^*$	0.2	5.49995×10^{-5}	0.00549501	0.00277542
	0.4	5.49992×10^{-5}	0.00549196	0.00277411
	0.6	5.49988×10^{-5}	0.00548791	0.00277255
	0.8	5.49979×10^{-5}	0.00547929	0.00276982

References

1. Eringen, A. C.: Theory of Micropolar Elasticity. In: Liebowitz, H., Ed., Fracture. Academic Press, New York, 621–729 (1968).
2. Cowin, S. C., An incorrect inequality in micropolar elasticity theory. J. appl. Math. Phys. **21**, 1970, 494–497.
3. Yang, J. F. C., Lakes, R. S., Transient study of couple stress in compact bone: torsion. J. Biomech. Engng. **103**, 1981, 275–279.
4. Yang, J. F. C., Lakes, R. S., Experimental study of micropolar and couple-stress elasticity in bone in bending. J. Biomech. **15**, 1982, 91–98.
5. Lakes, R., Nakamura, S., Behiri, J., Bonfield, W., Fracture mechanics of bone with short cracks. J. Biomech., **23**, 1990, 967–975.
6. Park, H. C., Lakes, R. S., Fracture mechanics of bone with short cracks. J. Biomech., **23**, 1987, 967–975.
7. Lakes, R., Materials with structural hierarchy. Nature, **361**, 1993, 511–515.

8. Tanaka, M., Adachi, T.: Lattice continuum model for bone remodeling considering microstructural optimality of trabecular architecture. In: Pedersen, P., Bendsoe, M.P. (Eds.), *Proceedings of the IUTAM Symposium on Synthesis in Bio Solid Mechanics*, Kluwer Academic Publishers, The Netherlands, 43–54 (1999).
9. Fatemi, J., Van Keulen, F., Onck, P.R., Generalized continuum theories: application to stress analysis in bone. *Meccanica*, **37**, 2002, 385–396.
10. Fatemi, J., Onck, P.R., Poort, G., Van Keulen, F., Cosserat moduli of anisotropic cancellous bone: a micromechanical analysis. *J. Phys. IV France.*, **105**, 2003, 273–280.
11. Goda, I., Assidi, M., Belouettar, S., Ganghoffer, J. F., Fracture mechanics of bone with short cracks. *J. Biomech.*, **23**, 1990, 967–975.
12. Jasiuk, I., in *Micromechanics of Bone Modeled as a Composite Material*, ed. by Meguid, S., Weng, G. *Micromechanics and Nanomechanics of Composite Solids*. Springer, Cham, 2018.
13. Sack, K. L., Skatulla, S., Sansour, C., Biological tissue mechanics with fibres modelled as one-dimensional Cosserat continua. Applications to cardiac tissue. *Int. J. Solids Struct.*, **81**, 2016, 84–94.
14. Hussan, J. R., Trew, M. L., Hunter, P. J., A mean-field model of ventricular muscle tissue. *J. Biomech. Eng.* **134**(7), 2012, 071003.
15. Adhikary, D.P., Dyskin, D.V., A Cosserat continuum model for layered materials. *Computers and Geotechnics*, **20**(1), 1997, 1545.
16. Riahi, A., Curran, J.H., Full 3D finite element Cosserat formulation with application in layered structures. *Applied Mathematical Modelling* **33**, 2009, 3450–3464.
17. Lebée, A., Sab, K., A Cosserat multiparticle model for periodically layered materials. *Mechanics Research Communications* **37**, 2010, 293–297.
18. Riahi, A., Curran, J.H., Full 3d finite element Cosserat formulation with application in layered structures. *Appl. Math. Modell.*, **33**, 2009, 3450–3464.
19. Riahi, A., Curran, J.H., Comparison of the Cosserat continuum approach with finite element interface models in a simulation of layered materials. *Trans. A: Civ. Eng.*, **17**(1), 2010, 39–52.
20. Nika, G., On a hierarchy of effective models for the biomechanics of human compact bone tissue. HAL Id: **hal-03629864**.
21. Bigoni, D., Drugan, W., Analytical derivation of Cosserat moduli via homogenization of heterogeneous elastic materials. *J. Appl. Mech.* **74**(4), 2007, 741–753.
22. Forest, S., Sab, K., Cosserat overall modeling of heterogeneous media. *Mech. Res. Commun.* **25**(4), 1998, 449–454.
23. Forest, S., Padel, F., Sab, K., Asymptotic analysis of heterogeneous Cosserat media. *Int. J. Solids Struct.* **38**, 2001, 4585–4608.
24. Forest, S., Trinh, D., Generalized continua and non-homogeneous boundary conditions in homogenisation methods. *J. Appl. Math. Mech. ZAMM* **91**(2), 2011, 90–109.
25. Gorbachev, V.I., Emel’yanov, A.N. Homogenization of the Equations of the Cosserat Theory of Elasticity of Inhomogeneous Bodies. *Mech. Solids*, **49**(1), 2014, 73–82.
26. Gorbachev, V., Emel’yanov, A., Homogenization of problems of Cosserat theory of elasticity of composites. Additional materials. In: *Intern. Scientific Symposium in Problems of Mechanics of Deformable Solids Dedicated to A.A. Il’Yushin on the Occasion of his 100th Birthday* **49**, 2021, 81–88, [in Russian].
27. Bövik, P., On the modelling of thin interface layers in elastic and acoustic scattering problems. *Q. J. Mech. Appl. Math.*, **47**(1), 1994, 17–42.
28. Ensan, M., Nejad., Shahrour, I., A macroscopic constitutive law for elasto-plastic multilayered materials with imperfect interfaces: application to reinforced soils. *Comput. Geotech.*, **30**, 2003, 339–345.
29. Duong, V. A., Diaz Diaz, A., Chataigner, S., Caronn, Jean-François. A layerwise finite element for multilayers with imperfect interfaces. *Compos. Struct.*, **93**, 2011, 3262–3271.

30. Sertse, H., Yu, W., Three-dimensional effective properties of layered composites with imperfect interfaces. *Adv. Aircr. Spacecr. Sci.* **4(6)**, 2017, 639—650.
31. Khoroshun, L.P., Effective Elastic Properties of Laminated Composite Materials with Interfacial Defects. *Int. Appl. Mech.* **55**, 2019, 187–198.
32. Brito-Santana, H., Christoff, B.G., Mendes Ferreira, A.J., Lebon, F., Rodríguez-Ramos, R., Tita, V., Delamination influence on elastic properties of laminated composites. *Acta Mech.*, **230**, 2019, 821–837.
33. Achenbach, J.D., Zhu, H., Effect of interfacial zone on mechanical behavior and failure of fiber-reinforced composites. *J. Mech. Phys. Solids.* **37(3)**, 1989, 381–393.
34. Hashin, Z., Thin interphase/imperfect interface in elasticity with application to coated fiber composites. *J. Mech. Phys. Solids.* **50(12)**, 2002, 2509—2537.
35. Videla, J., Atroshchenko, E., Analytical study of a circular inhomogeneity with homogeneously imperfect interface in plane micropolar elasticity. *Z. Angew. Math. Mech.* **97(3)**, 2017, 322–339.
36. Ciarlet, P.G., *Mathematical Elasticity, vol. II: Theory of Plates.* North-Holland, Amsterdam, 1997.
37. Geymonat, G., Hendili, S., Krasucki, F., Serpilli, M., Vidrascu, M., Asymptotic Expansions and Domain Decomposition. In: Erhel, J., Gander, M., Halpern, L., Pichot, G., Sassi, T., Widlund, O. (eds) *Domain Decomposition Methods in Science and Engineering XXI. Lecture Notes in Comput. Sci. Eng.*, **98**. Springer, Cham, 2014.
38. Serpilli, M., Krasucki, F., Geymonat, G., An asymptotic strain gradient Reissner-Mindlin plate model. *Meccanica.* **48(8)**, 2013, 2007-2018.
39. Serpilli M., On modeling interfaces in linear micropolar composites. *Math. Mech. Solids.* **23(4)**, 2018, 667–685.
40. Serpilli, M.: Classical and higher order interface conditions in poroelasticity. *Ann. Solid Struct. Mech.* **11**, 2019, 1—10.
41. Serpilli, M., Rizzoni, R., Rodríguez-Ramos, R., Lebon, F., Dumont, S. A novel form of imperfect contact laws in flexoelectricity. *Comp. Struct.* **300**, 2022, 116059.
42. Yanes, V., Sabina, F. J., Espinosa-Almeyda, Y., Otero, J. A., Rodríguez-Ramos, R., in *Asymptotic homogenization approach applied to Cosserat heterogeneous media*, ed. by Andrianov, I., Gluzman, S., Mityushev, V. *Mechanics and Physics of structured media.* Academic Press, Elsevier, USA, 2022.
43. Rodríguez-Ramos, R., Yanes, V., Espinosa-Almeyda, Y., Otero, J. A., Sabina, F. J., Sánchez-Valdés, C. F., Lebon, F., Micro-macro asymptotic approach applied to heterogeneous elastic micropolar media. Analysis of some examples. *Int. J. Solids Struct.*, **239-240**, 2022, 111444.
44. Rubin, M.B., Benveniste, Y., A Cosserat shell model for interphases in elastic media. *J. Mech. Phys. Solids*, **52(5)**, 2004, 1023–1052.
45. Dong, H., Wang, J., Rubin, M., Cosserat interphase models for elasticity with application to the interphase bonding a spherical inclusion to an infinite matrix. *Int. J. Solids Struct.*, **51(2)**, 2014, 462–477.
46. Dong, H., Wang, J., Rubin, M., A nonlinear cosserat interphase model for residual stresses in an inclusion and the interphase that bonds it to an infinite matrix. *Int. J. Solids Struct.*, **62**, 2015, 186–206.
47. Kumari, R., Singh, A. K., Chaki, M. S., Influence of Abrupt Thickening on the Shear Wave Propagation on Reduced Cosserat Media with Imperfect Interface. *Int. J. Geomech.*, **22(4)**, 2022, 04022018.
48. Espinosa-Almeyda, Y., Yanes, V., Rodríguez-Ramos, R., Sabina, F.J., Lebon, F., Sánchez-Valdés, C.F., Camacho-Montes, H., Chapter 6: Overall properties for elastic micropolar heterogeneous laminated composites with centro-symmetric constituents. In book series *Advanced Structured Materials 8611, Mechanics of High-Contrast Elastic Solids: Contributions from*

- Euromech Colloquium 626. Editor: Prof. Holm Altenbach, Dr. Danila Prikazchikov, Prof. Andrea Nobili. Springer, 2022 (in press).
49. Eringen, A. C.: *Microcontinuum Field Theories I: Foundations and Solids*. Springer, New York (1999).
 50. Sanchez-Palencia, E.: *Non-Homogeneous Media and Vibration Theory*. Berlin, Springer Berlin, Heidelberg, (1980).
 51. Pobedrya, B.: *Mechanics of Composite Materials* (in Russian), First edition, Moscow, Izd-vo MGU, (1984).
 52. Bakhvalov, N., Panasenko, G.: *Homogenization: Averaging Process in Periodic Media*. In *Mathematics and Its Applications (Soviet Series)*, First edition, Moscow, Lenin Hills, (1989).
 53. Hassanpour, S., Hepler, G. R. Micropolar elasticity theory: a survey of linear isotropic equations, representative notations, and experimental investigations. *Math. Mech. Solids* , **22**, 2017, 224–242.
 54. Dunn, M., Ledbetter, H. Poisson's ratio of porous and microcracked solids: Theory and application to oxide superconductors. *J. Mater. Res.*, **10(11)**, 1995, 2715–2722.